# Improved airfoil polar predictions with data-driven boundary-layer closure relations

De Oliveira, Gael; Pereira, Ricardo; Timmer, Nando; Van Rooij, Ruud

**Important note**
To cite this publication, please use the final published version (if applicable).
Please check the document version above.

**PAPER • OPEN ACCESS**

# Improved airfoil polar predictions with data-driven boundary-layer closure relations

To cite this article: Gael de Oliveira *et al* 2018 *J. Phys.: Conf. Ser.* **1037** 022009

View the article online for updates and enhancements.
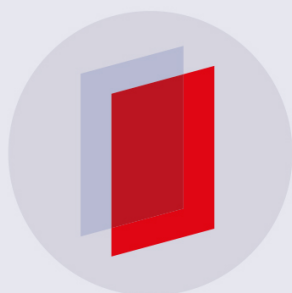
**IOP ebooks™**

Bringing you innovative digital publishing with leading voices to create your essential collection of books in STEM research.

Start exploring the collection - download the first chapter of every title for free.

# Improved airfoil polar predictions with data-driven boundary-layer closure relations

**Gael de Oliveira, Ricardo Pereira, Nando Timmer, Ruud van Rooij**

Aerospace Faculty, Delft University of Technology, Kluyverweg 1, 2629HS Delft, Netherlands

E-mail: `g.l.deoliveiraandrade@tudelft.nl`

**Abstract.** The accuracy of airfoil polar predictions is limited by the usage of imperfect turbulence models. Can machine-learning improve this situation? Will airfoil polars teach the effect of turbulence on skin-friction? We try to answer these questions by refining turbulence treatment in the Rfoil code: boundary layer closure relations are learned from airfoil polar data. Two turbulent closure relations, for skin friction and energy shape factor, are parametrized with a class-shape transformation. An experimental database is then used to define code inaccuracy measures that are minimized with an interior point gradient algorithm. Results show that airfoil polars contain exploitable information about turbulent phenomena. Inferred closures agree with direct numerical simulation results of skin friction and the new code predicts drag more accurately. Maximum lift remains under-predicted but Rfoil maintains its robustness and suitability for optimization of wind energy airfoils.

## 1. Introduction

Wind turbine airfoils operate in high Reynolds flows with intricate eddies that cannot be resolved in practical simulations. Flow solvers model the effect of unresolved turbulent phenomena by combining mechanistic insight with closure relations. Closures inject empirical knowledge into simulations and dominate errors in airfoil predictions [1–3] – be it for Viscous-Inviscid (VII) [4,5], Reynolds Averaged Navier-Stokes (RANS) [6], Large-Eddy (LES) [7] or Lattice-Boltzman [8] environments. But good closures matter: less uncertainty means better design optimization and lower cost of wind energy [9].

Current understanding of turbulence is shaped by a century of dialogue between statistic [10–13], structural [14, 15], and deterministic [16, 17] perspectives [18, 19]. But advances in turbulence thinking have limited impact on engineering approaches despite industrial demand [6, 20, 21]; and direct numerical simulations (DNS) of high Reynolds flows are still two decades from maturity [22]. How can models improve until then? Tracey [23, 24], Durasaimy [25, 26] and Ling [27, 28] are advocating for data-driven approaches: using minimization algorithms to learn turbulent closures from high-fidelity simulations and experimental data [21,29,30]. Results for RANS [31–34] and LES [35–37] frameworks are encouraging, but applications of machine-learning to viscous-inviscid frameworks remain sparse.

Can data teach the effect of turbulence on skin-friction? Are airfoil polars exploitable for this purpose? Viscous-inviscid interaction (VII) codes like Rfoil [5] and Xfoil [4] are ideal to answer these questions: they have modest computational requirements, take a structural view on turbulence, and use the $e^N$ method [38] to predict laminar-turbulent transition accurately [2,39].

| $\delta^*$ | $= \int_0^\infty \left(1 - \frac{U}{U_e}\right) dy$ | Displacement Thickness | $H$ | $= \frac{\delta^*}{\theta}$ | Shape Factor |
|---|---|---|---|---|---|
| $\theta$ | $= \int_0^\infty \frac{U}{U_e}\left(1 - \frac{U}{U_e}\right) dy$ | Momentum Thickness | $H^*$ | $= \frac{\delta^{**}}{\theta}$ | Energy Factor |
| $\delta^{**}$ | $= \int_0^\infty \frac{U}{U_e}\left(1 - \frac{U^2}{U_e^2}\right) dy$ | Energy Thickness | $C_f$ | | Friction Coeff. |
| $Re_\theta$ | $= \frac{U_e\theta}{\nu}$ | Momentum Reynolds | $C_D$ | | Dissipation Coeff. |

**Table 1.** Integral boundary layer variables (see reference [43] for detailed definitions)

That is why we use experimental airfoil polars to learn new turbulent closure relations for the Rfoil code. Section 2 reviews Rfoil's error sources to identify machine-learning opportunities. Section 3 describes the supervised learning method: it is crude by modern standards and does not use neural networks. Results comprise a tailored Rfoil code and closure relations for turbulent skin friction ($C_f$) and energy shape factor ($H^*$). Section 4 checks the physical consistency of the new closures and their impact on polar predictions.

## 2. Boundary layer treatment in Rfoil

Rfoil is derived from Xfoil and solves an approximate form of the Navier-Stokes (NS) equations obtained by truncating a matched asymptotic expansion [40, 41]. The outer expansion concerns convectively-dominated flow in the far field whereas the inner expansion deals with shear-flow near the airfoil surface. Outside deep-stall, the inner flow is approximately governed by the boundary-layer partial-differential-equations (BL-PDE) [41, 42]:

$$\begin{cases} U\frac{\partial U}{\partial x} + V\frac{\partial U}{\partial y} = -\frac{1}{\rho}\frac{\partial P}{\partial x} + \nu\left(\frac{\partial^2 U}{\partial y^2}\right) \\ \nabla \cdot \boldsymbol{U} = 0 \qquad \wedge \qquad \frac{\partial P}{\partial y} = 0 \end{cases} \quad with \quad BCs = \left\{ \begin{array}{c} \text{prescribed } U_e \\ \text{edge velocity} \end{array} \right\} \tag{1}$$

The boundary-layer (BL) flow is solved with an integral method based on the Von Karman equations [41, 43]:

$$\begin{cases} \frac{\partial \theta}{\partial x} = \frac{C_f}{2} - (H_{12} + 2)\frac{\theta}{U_e}\frac{\partial U_e}{\partial x} \\ \frac{\partial H_{32}}{\partial x} = \frac{2C_D}{\theta} - \frac{H_{32}}{\theta}\frac{C_f}{2} + (H_{12} - 1)\frac{H_{32}}{U_e}\frac{\partial U_e}{\partial x} \end{cases} \quad with \quad BCs = \left\{ \begin{array}{c} \text{prescribed} \\ U_e = f_{(X)} \end{array} \right\} \tag{2}$$

These equations (2) are obtained by integrating the BL-PDEs (1) analytically in the normal direction ($x$). No approximations are involved in this procedure. But while the BL-PDEs (1) are closed, system (2) comprises two ordinary differential equations (ODEs) that depend on five variables (see table 1 for notation). Solving system (2) therefore requires additional connections between variables, and these are known as closure relations.

### 2.1. Laminar and turbulent closure relations

Rfoil resorts to different closure relations for each flow region – laminar BL, turbulent BL and wake. Transition between flow regions is predicted with a supplementary ODE for the growth of Tollmien-Schlichting waves [38] and matching laws are used at interfaces – near stagnation, laminar-turbulent transition and the trailing edge.

Laminar closure relations are backed by solid theory [44]. Similarity conditions allow the construction of two-state velocity profiles [45, 46] that originate accurate closure datasets [47]. These closures are only exact for specific pressure histories [48] but laminar flows have limited memory. Departure from similarity has negligible effects in the absence of turbulent eddies [49].

The theory of turbulent closure relations is weaker [50–52]. Rfoil uses two-state closures for turbulent skin friction ($C_f$) and energy factor $H^*$:

$$C_f^{org} = f_{(H, Re_\theta)} \qquad , \qquad H^{*org} = f_{(H, Re_\theta)} \tag{3}$$
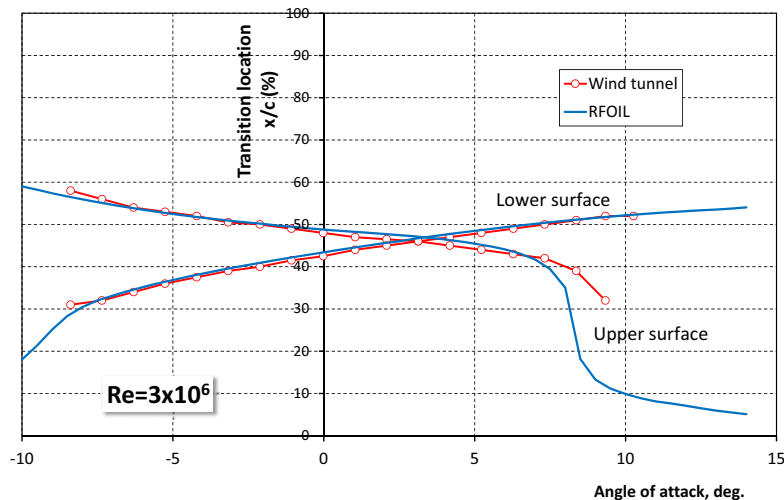
**Figure 1.** Transition location on a 24% thick airfoil measured in TU-Delft's LTT.

Bivariate closures of this kind assume Clauser equilibrium [53] but airfoil pressure histories [54, 55] often drive flow away from equilibrium [56, 57]. Turbulent boundary layers require additional descriptors for history effects, and that is acknowledged with the shear-lag equation:

$$\frac{\delta}{C_\tau}\frac{\partial C_\tau}{\partial x} = K_C \left( C_\tau^{\frac{1}{2}} - C_{\tau_{EQ}}^{\frac{1}{2}} \right) + \left\{ \begin{array}{c} \text{diffusive} \\ \text{terms} \end{array} \right\} \tag{4}$$

This ODE adds a state related to flow memory, the turbulent shear stress coefficient ($C_\tau$). It is derived from Green's approximation [58] of Bradshaw's equation [59] for the transport of turbulent kinetic energy; and enables computation of the dissipation coefficient ($C_D$) with a ($C_\tau$) that lags behind equilibrium values ($C_\tau^{eq}$) inferred from the Clauser $G - \beta$ relation [60, 61].

$$G = A\sqrt{1 + B\beta} \tag{5}$$

But the shear-lag approach is attackable [1, 62]: it depends on a shear stress profile that contradicts experimental evidence [56, 57], its diffusive term is debated [61, 62] and the $K_C$ factor encompasses substantial uncertainty [5].

*2.2. Sources of prediction error*
Accurate load predictions require accurate closures at every flow stage, and the mechanistic arguments of section 2.1 suggest that turbulent closures are the greatest source of error. Rfoil underestimates drag in most conditions [63], and the issue is greatest on airfoils with short laminar runs. Longer turbulent runs seem to correlate with to greater drag underprediction.

Accurate prediction of the transition location requires accurate flow solutions of every flow region but the turbulent boundary layer and wake. And Rfoil predicts transition accurately, as can be seen on the illustrative case of figure .. . That case corresponds to an airfoil with 24% thickness measured in TU-Delft's LTT, and it provides experimental evidence for the problematic nature of Rfoil's turbulent closures.

Airfoil designers circumvent turbulence modeling shortcommings with various workarounds. Some designers tailor the $G - \beta$ relation (5) to specific cases, others use custom skin-friction relations (3), and yet others correct the polar curve directly. Typical corrections depend on airfoil thickness, leading-edge radius, extent of laminar run or Reynolds number [63]. Semi-empirical correction methods suggest airfoil polar data can reveal systematic trends that remain unexploited by closure relations.

3

*2.3. Machine learning opportunities*

Unexploited information and epistemic uncertainty signal machine-learning opportunities. But what exactly is machine-learning? According to Mitchell [64]:

> *"A computer program is said to learn from experience E with respect to some class of tasks T and performance measure P, if its performance at tasks in T, as measured by P, improves with experience."* [64]

Think of a task ($T$) that consists in predicting airfoil polars. Learning could use experience ($E$, predictions with different settings) to modify a flow solver (*Rfoil*) in ways that improve its performance ($P$, accuracy against reference results).

Such a setup is typical of supervised-learning and could be used to improve several terms in Rfoil's turbulent closure:

 (i) Matching rules at boundary layer interfaces

 (ii) Shape and coefficients of the $G - \beta$ closure relation (5)

(iii) Diffusive terms and slip-velocity closure of the shear-lag equation (4)

(iv) Enhanced skin friction ($C_f$) and energy shape-factor ($H^*$) closure relations (3)

The present contribution narrows its scope to the last, and simplest, option of the above list.

## 3. Supervised learning of closure relations

We use airfoil polar data to learn new closure relations for turbulent skin friction ($C_f$) and energy shape-factor ($H^*$). The two-state dependency $f(H, Re_\theta)$ is maintained despite its shortcomings and the new closures are defined parametrically.

$$C_f^{learn} = f_{\left(H, Re_\theta; \psi^{cf}\right)} \qquad , \qquad H^{*learn} = f_{\left(H, Re_\theta; \psi^*\right)} \tag{6}$$

Learning consists in finding parameters ($\psi$) that lead to improved closure relations. But what are better closures? Traditional approaches [43,53] emphasize agreement with detailed boundary layer measurements. Recent work [1, 5, 24] defends that better closure relations lead to better flow predictions. The two definitions are not contradictory and we assume they correlate well. The outcomes of the learning process will tell if that holds true.

Formally, we seek to learn by minimizing the expectation ($\mathbb{E}$) of a measure for Rfoil's inaccuracy ($\mathcal{L}$) in the prediction of airfoil polar curves ($f_{(\boldsymbol{x}, \beta)}^p$). The problem is formalized after Goodfellow [65]:

$$\min_{\psi} \quad \mathbb{E}_{(\boldsymbol{x}, \boldsymbol{y}) \sim p_{data}} \mathcal{L}\left(f_{(\boldsymbol{x}, \psi)}^p, \boldsymbol{y}\right) \qquad \approx \qquad \min_{\psi \in D} \quad \frac{1}{m} \sum_{i=1}^{i=m} \mathcal{L}\left(f_{(\boldsymbol{x}_i, \psi)}^p, \boldsymbol{y}_i\right) \tag{7}$$

Experimental reference ($\boldsymbol{y}$ - reference aerodynamic coefficients) and conditions ($\boldsymbol{x}$ - airfoil coordinates, Mach, Reynolds) would ideally span the entire data generating distribution ($p_{data}$) of the physical world. This is impossible, so the expected inaccuracy norm of Rfoil's polar predictions is approximated over a discrete collection $\{\boldsymbol{x}_i, \boldsymbol{y}_i\}$ of $i = 1...m$ of experimental samples.

*3.1. Experimental reference*

Reference data is sampled from airfoil polar curve measurements of Abbot and Van Doenhoff [66]. A database was constructed using digitized data [67] from the NACA TR824 report [66] that spans several 4, 5 and 6 digit NACA airfoils. Reynolds numbers range from 3 to 9 million and airfoil coordinates were regenerated with the NACA456 code [68]. Rough leading edge and thin airfoil ($t/c < 0.1$) cases were excluded to limit overcompensation risks. Aerodynamic coefficients were reinterpolated into $C_l - \alpha$ , $C_d - \alpha$ and $C_m - \alpha$ curves but the data was left uncorrected to ease reproducibility.

### 3.2. Inaccuracy measure

Inaccuracy is measured with a combination of least square error norms that confront Rfoil's predictions with a training datased sampled from the experimental reference. The global inaccuracy measure $\mathcal{L} = f_{(\psi)}$ is a scalar that combines topical error norms for lift, drag and moment coefficients.

Norms for each coefficient ($\mathcal{L}^{C_l}$, $\mathcal{L}^{C_d}$ and $\mathcal{L}^{C_m}$) are scaled with reference values $\left(\mathcal{L}^{C_{\cdots}}_{ref}\right)$ computed at the beginning of the learning process.

$$\mathcal{L} = \left(\frac{\mathcal{L}^{C_l}}{\mathcal{L}^{C_l}_{ref}}\right)^2 + \left(\frac{\mathcal{L}^{C_d}}{\mathcal{L}^{C_d}_{ref}}\right)^2 + \left(\frac{\mathcal{L}^{C_m}}{\mathcal{L}^{C_m}_{ref}}\right)^2 \tag{8}$$

Coefficient norms $\left(\mathcal{L}^{C_{\cdots}}\right)$ are computed separately for each aerodynamic coefficient and combine inaccuracy measures from all experimental cases $\left(\mathcal{L}^{C_{\cdots}}_i\right)$ in the training set:

$$\mathcal{L}^{C_{\cdots}} = \left(\frac{1}{m}\sum_{i=1}^{i=m}\left(\mathcal{L}^{C_{\cdots}}_i\right)^2\right)^{\frac{1}{2}} \tag{9}$$

Each experimental case represents a unique combination of airfoil and Reynolds number. Case inaccuracy norms $\left(\mathcal{L}^{C_{\cdots}}_i\right)$ consist in the root mean square integral of the difference between predicted ($C^{num}_{\cdots}$) and measured ($C^{exp}_{\cdots}$) aerodynamic coefficients over the range of experimental angles of attack ($\alpha$):

$$\mathcal{L}^{C_{\cdots}}_i = \left(\frac{\int\left(C^{num.}_{\cdots(\boldsymbol{x}_i,\psi)} - C^{exp.}_{\cdots(\boldsymbol{x}_i)}\right)^2 d\alpha}{\int d\alpha}\right)^{\frac{1}{2}} \tag{10}$$

### 3.3. Parametric closure relations

Closure relations are parametrized with a variant of the Class Shape Transformation (CST) [69]. The idea consists in using a shape function ($S^{dM}$) that modifies the original closure relations ($C^{org}_f$ and $H^{*org}$) in arbitrary ways:

$$
\begin{aligned}
C^{learn}_{f\left(H,Re_\theta,\psi^{cf}_i\right)} &= S^{dM}_{\left(H,\psi^{cf}_i\right)}\left(C^{org}_{f(H,Re_\theta)} + \delta^{C_f}\right) - \delta^{C_f} \quad &with \quad &\delta^{C_f} = 0.004 \\
H^{*learn}_{\left(H,Re_\theta,\psi^*_i\right)} &= S^{dM}_{\left(H,\psi^*_i\right)}\left(H^{*org}_{(H,Re_\theta)} + \delta^{H^*}\right) - \delta^{H^*} \quad &with \quad &\delta^{H^*} = 0
\end{aligned}
$$

The $S^{dM}$ function is constructed by linear combination of the $M^{th}$ degree Bernstein polynomial basis. Its behavior is controlled by $M+1$ parameters ($\psi^{cf}_i, \psi^*_i \in \mathbb{R}^{M+1}$):

$$S^{dM}_{(H,\theta_i)} = \begin{cases} A_0 & 0 < \eta_{(H)} \\ \sum_{i=0}^{i=M}\theta_{i+1}B^{Mi}_{(\eta_{(H)})} & 0 < \eta_{(H)} < 1 \\ A_{M+1} & 1 < \eta_{(H)} \end{cases} \quad with \quad \begin{cases} B^{Mi}_{(x)} = \begin{pmatrix} M \\ i \end{pmatrix} x^i \left(1-x\right)^{M-i} \\ \eta_{(H)} = \frac{H - H_{lb}}{H_{ub} - H_{lb}} \end{cases}$$

Closure relation modifications are confined to a relatively narrow interval $[H_{lb}, H_{ub}]$ of shape factors. The lower bound is set at the vanishing boundary layer limit ($H_{lb} = 1$) and the upper bound corresponds to separated flow ($H_{ub} = 6$). Two constraints are enforced:
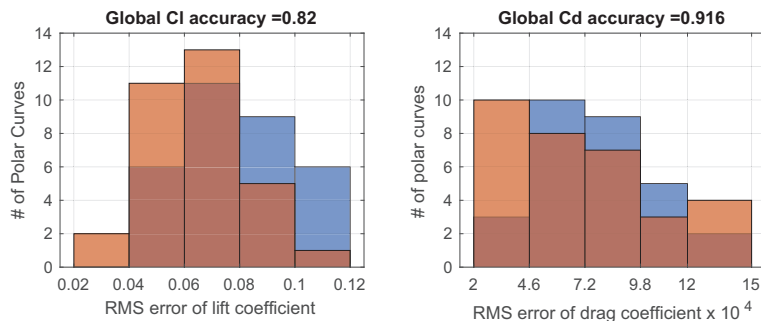
**Figure 2.** Effect of learning on standard deviation of lift and drag predictions over training set.

(i) First derivative discontinuities at the upper bound are limited by aggregating the last shape parameters ($\psi_M^{cf} = \psi_{M+1}^{cf}$ and $\psi_M^* = \psi_{M+1}^*$)

(ii) Original closure relation values at the vanishing boundary layer limit are maintained ($\psi_1^{cf} = \psi_1^* = 1$) to preserve asymptotic behavior

Bernstein polynomials of very modest order ($M + 1 = 6$) were used, but these shape functions allow progressive refinement across multivariate polynomial spaces and the generality of the method can be proven [69].

We hope these choices will not mislead readers into considering the CST method overly restrictive. Shape functions can be designed to allow progressive refinement across multivariate polynomial spaces and the generality of the method can be proven [69].

*3.4. Solution algorithm*
Closure relations are learned by changing the parameters until the inaccuracy norm is minimized. This is achieved with a gradient descent algorithm based on the interior point method [70,71]: the algorithm starts from the original closures ($\boldsymbol{\psi}_i^{cf} = \boldsymbol{\psi}_i^* = 1\,, \forall i$) and combines conjugate gradient steps with line search iterations to find sensible moves [71]. Gradients are estimated with fixed-step central differences, the hessian matrix is approximated through the dense BFGS method[] and numerical noise is carefully attenuated. Together with a parsimonious parametrization and tractable dataset, these measures enable the obtention of formally converged minima.

## 4. Results and Discussion
The minimization algorithm reduced the scalar inaccuracy measure (8) from an initial value of $\sqrt{3} \approx 1.7321$ to 1.5725. Coefficient accuracy measures, defined in expression 9, improved for all three aerodynamic coefficients:

| | | Before learning | After learning | Improvement |
|---|---|---|---|---|
| Lift innacuracy measure | $\mathcal{L}^{C_l}$ | 0.0813 | 0.0667 | 18.0% |
| Drag innacuracy measure | $\mathcal{L}^{C_d}$ | 8.7649e-04 | 8.0302e-04 | 8.40% |
| Moment innacuracy measure | $\mathcal{L}^{C_m}$ | 0.0178 | 0.0174 | 1.90% |

The training dataset comprised 1524 datapoints spread over 33 experimental cases for NACA 4-series airfoils with relative thickness above 10%. Innacuracy measures improved differently for each experimental case and figure 2 shows histograms of drag and lift prediction errors at the case level, as given by expression 10. Learning shifted the error histograms to the left and that is desirable. The drag innacuracy measure improved for all but two cases in the training set. The two spurious points of the drag histogram correspond to situations in which Rfoil predicted
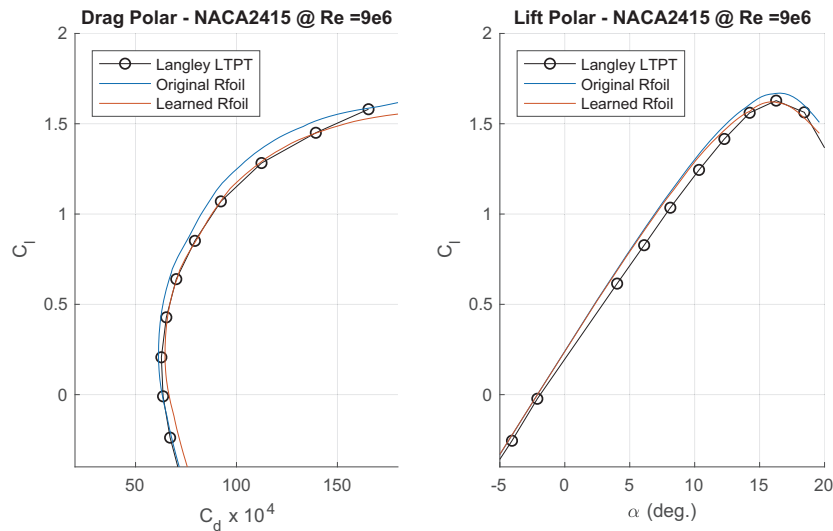
**Figure 3.** Effect of learning on polar prediction for airfoil in training set.

transition too early. The width of the laminar drag bucket was then underestimated, and led to a paradoxal situation in which turbulence model improvements degraded the overall drag accuracy measure.

Future efforts might resolve the above artifact by selecting the transition threshold more carefully. The present work used a critical amplification factor of $N = 9$ for all simulations, but different values are probably more appropriate for the Langley LTPT tunel.

*4.1. Effect on Polar Predictions*
Polar predictions improved in qualitative terms for all airfoils in the training set. Figure 3 shows the effect of learning on the NACA2415 airfoil at a Reynolds number of 9 million. Rfoil's traditional drag under-prediction was attenuated and maximum-lift approached the experimental reference. Differences in the slope of the lift curve remained throughout the learning process but that is probably due to experimental shortcommings: early lift measurements in the Langley LTPT were obtained by integrating wall pressures over a small number of orifices. Combined with primitive correction methods, that probably lead to systematic understimation of the lift curve slope [63].

Figure 4 compares polar curves for the DU96-W180 airfoil at a Reynolds number of 3e6, as measured in TU-Delft's Low Turbulence Tunnel (LTT) [72]. Improvements in drag prediction are clear and suggest that learning enhanced the predictive power of Rfoil: the DU96-W180 case functions as a verification because it did not belong to the training set.

Maximum-lift predictions deteriorated slightly for the verification case. The origin of underpredictions in maximum-lift is still misunderstood: it could be due to biases in the training set, over-compensation, under-fitting, or simply the price to pay for better drag predictions. Future efforts can elucidate these hypotheses by using more dependable datasets and by allowing wider modifications in Rfoil's turbulent closure.

*4.2. Learned Closure Relations*
Figure 5 shows the effect of learning on closure relations. A modest momentum Reynolds number was chosen to enable comparison with the closures of the Eppler airfoil prediction code [73].Even if these changes had substantial effect on polar predictions, they remained within the range of uncertainty associated with historical boundary layer measurements [43].
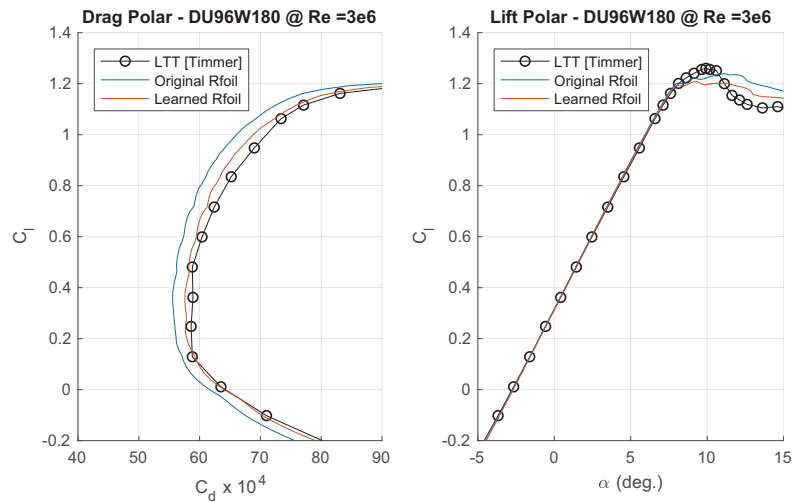
**Figure 4.** Effect of learning on polar prediction for airfoil outside training set.
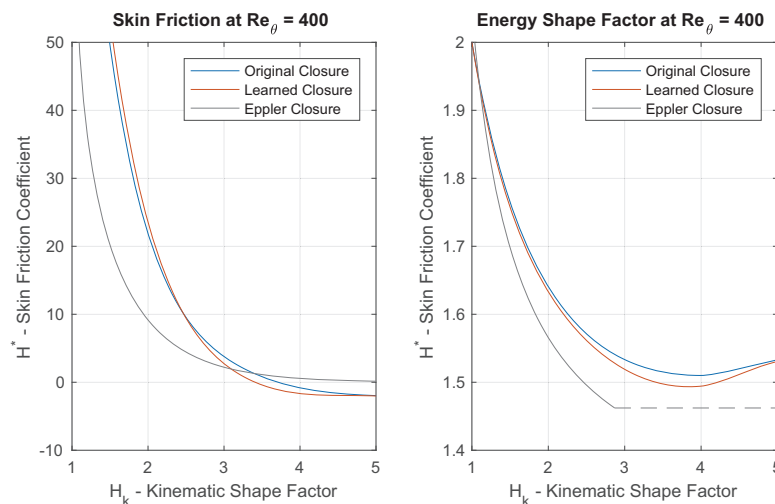


**Figure 5.** Learned skin friction and $H^*$ closures compared to original Rfoil and Eppler code closures.

The new closure predicts higher skin friction values than the original one. This makes sense because older boundary layer studies [53, 60] underestimated skin friction in adverse pressure gradients: skin friction was traditionally estimated by extrapolation pitot or hot-wire measurements with incorrect law-of-the-wall assumptions [56, 57, 74]. Oil film interferometry measurements and direct numerical simulations (DNS) do not depend on law of the wall assumptions, and produce higher skin friction estimates that thought to be more accurate.

Figure 6 compares the learned skin friction closure with a recent DNS result published by Vinuesa et al. [75]. Agreement also improves for the other datapoints published of reference [75]. Improved agreement of closure relations with detailed BL data seems to correlate well with improvements in airfoil polar prediction, as we had hoped in the beginning of section 3. The effects of turbulence on skin friction can indeed be learned from airfoil polar data.

### 4.3. Learning exercises
Several learning exercises were conducted to understand the effect of different training sets, performance norms and algorithm settings. Variations in the learning method did not affect learning outcomes in substantial ways, and lead to the following insights:
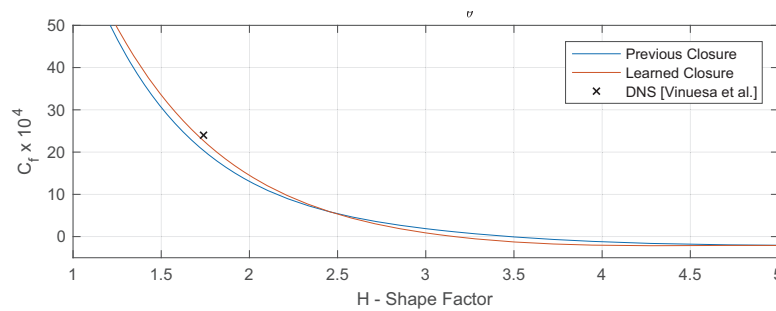
**Figure 6.** Comparison of learned skin friction closure with DNS data of Vinuesa et al. [75].

- **Inaccuracy norm:** The approach described here provides stable gradients and agrees well with heuristic understandings of code accuracy. Most importantly, it uses all available data points. This may appear inefficient because some data points hold limited information about what we want to learn. Think of lift measurements in the linear region: we know what they should be and already trust our codes on this matter. But these points are important for machine-learning because they teach what we don't want to forget.

- **Parametric representation**: The current parametrization is restrictive and leads to some underfitting. Future studies should use more parameters by increasing the order of the $H$ parametrization, using a bivariate shape function that includes $Re_\theta$ effects, or accounting for equilibrium departure with a trivariate closure. Extension of the parametrization is straightforward, but broader design spaces are only advantageous if the training set contains sufficient information. We decided not to learn an $Re_\theta$ dependency from the TR824 dataset because its coverage of the data-generating distribution seemed too narrow: low $Re_\theta$ values are heavily correlated with low shape factors because all airfoils were measured at high chord Reynolds numbers.

- **Solution Algorithm**: Results obtained with different full batch deterministic gradient algorithms are similar. The learning problem (7) is formally non-convex but the original convergence basin seems wide and slightly shallow. Alternative convergence basins were identified with a simulated annealing algorithm [76] but these lead to narrow unphysical minima. Stochastic gradient (SGD) [65] algorithms are inefficient on small datasets [77] like the ones used here, but future studies should benefit from their scalability.

## 5. Final Note
Airfoil polars contain exploitable information about turbulent boundary layers. A relatively small dataset was able to teach a better skin friction closure to the Rfoil code. The new closure relation agrees with direct numerical simulation data that was not used for training, and leads to better drag predictions for airfoils inside and outside the training set. Lift predictions remained identical for the linear region but a decrease in maximum-lift estimations was observed. The extent to which this is desirable, or physically sound, remains unclear.

Reliable data is scarce, but it seems more important to learn from reliable data than from big data. When that holds true, turbulence learning will benefit from the use of parsimonious parametric representations. Variants of the CST parametrization could be appealing compared to neural-networks. CST methods are less general than modern machine-learning predictors, but that could be an advantage when the inaccuracy norm is computationally expensive and susceptible to robustness issues. Applications extend beyond viscous-inviscid interaction: future efforts can build on the current method to improve RANS or LES predictions of airfoil flows and wind turbine wakes.

## References

[1] Althaus D 1993 *Zeitschrift Flugwissenschaften and Weltraumförschung* **17** 253–256
[2] Sorensen N N, Mendez B, Munoz A, Sieros G, Jost E, Lutz T, Papadakis G, Voutsinas S, Barakos G, Colonia S, Baldacchino D, Baptista C and Ferreira C 2016 Cfd code comparison for 2d airfoil flows *Journal of physics and conference series* vol 753
[3] Sarlak H 2017 Large eddy simulation of an sd7003 airfoil: Effects of reynolds number and subgrid-scale modeling *Journal of physics: conference series* 854
[4] Drela M 1989 Xfoil: An analysis and design system for low reynolds number airfoils *Low Reynolds Number Aerodynamics* (*Lecture Notes in Engineering* no 54) (Springer-Verlag)
[5] van Rooij R 1996 Modification of the boundary layer calculation in rfoil for improved airfoil stall prediction Tech. rep. Delft University of Technology, Report IW-96087R
[6] Wilcox D 2006 *Turbulence modelling for CFD* (DCW Industries)
[7] Lu H and Rutland C J 2016 *Acta Mechanica Sinica*
[8] Sagaut P 2010 *Computers and mathematics with applications* **59**
[9] Abdallah I, Natarajan A and Sorensen J D 2015 *Renewable Energy* **75** 283–300
[10] Reynolds O 1894 *Philosophical Transactions of the Royal Society London A* **186**
[11] Prandtl L 1925 *Zeitschrift für angewandte Mathematik und Mechanik* **5** 136–139
[12] Taylor G 1935 *Proceedings of the Royal Society London A* **151** 421–478
[13] Tennekes H and Lumley J 1972 *A first course in turbulence* (MIT Press)
[14] Schubauer G and Skramstad H 1948 Laminar boundary-layer oscillations and transition on a flat plate Tech. rep. NACA Report 909
[15] Lumley J 1981 Coherent structures in turbulence *Transition and Turbulence* ed Meyer R (Academic Press) pp 215–242
[16] Lorenz E 1963 *Journal of the atmospheric sciences*
[17] Ruelle D 1981 *Bulletin of the American Mathematical Society*
[18] Chapman G and Tobak M 1985 Observations, theoretical ideas and modeling of turbulent flows - past, present and future Technical Memorandum 86679 Nasa
[19] McDonough J M 2007 Introductory lectures on turbulence Tech. rep. University of Kentucky, Dept. of Mech. Eng. and Math.
[20] Lesieur M 2008 *Turbulence in Fluids* (Springer Netherlands)
[21] Durbin P 2018 *Annual Review of Fluid Mechanics* **50** 77–103
[22] Slotnick J, Khodadoust A, Alonso J, Darmofal D, Gropp W, Lurie E and Mavriplis D 2014 Cfd vision 2030: A path to revolutionary computational aerosciences Tech. rep. NASA CR-2014-218178
[23] Tracey B, Durasaimy K and Alonso J 2013 Application of supervised learning to quantify uncertainties in turbulence and combustion modelling. *AIAA Aerospace Sciences Meeting*
[24] Tracey B, Durasaimy K and Alonso J 2015 A machine learning strategy to assist turbulence model development *53rd AIAA Aerospace Sciences Meeting*
[25] Durasaimy K, Singh A and Pan S 2017 Augmentation of turbulence models using field inversion and machine learning *55th AIAA Aerospace Sciences Meeting*
[26] Zhang Z and Durasaimy K Machine learning methods for data-driven turbulence modeling *AIAA Computational Fluid Dynamics Conf. 2015-2460*
[27] Ling J and Templeton J 2015 *Physics of Fluids* **27** 085103
[28] Ling J, Kurzawski A and Templeton J 2016 *Journal of Fluid Mechanics* **807** 155–166
[29] Kutz J N 2017 *Journal of Fluid Mechanics*
[30] Bose S and Park G 2018 *Annual Review of Fluid Mechanics* **50** 535–561
[31] Wang J, Wu J and Xiao H 2017 *Physical Review Fluids* **2** 034603
[32] Weatheritt J and Sandberg R 2017 *International Journal of Heat and Fluid Flow* **68** 298–318
[33] Singh A and Durasaimy K 2017 Characterizing and improving predictive accuracy in shock-turbulent boundary layer interactions using data-driven models *55th AIAA Aerospace Sciences Meeting*
[34] Singh A, Matai R, Durasaimy K and Durbin P 2017 Data-drive augmentation of turbulence models for adverse pressure gradient flows *23rd AIAA Computational Fluid Dynamics Conference*
[35] Barone M, Fike J, Chowdhary K, Ling J and Martin S 2017 Machine learning models of errors in large eddy simulation predictions of surface pressure fluctuations *47th AIAA Fluid Dynamics Conference*
[36] Maulik R and San O 2017 *Journal of Fluid Mechanics* **831** 151–181
[37] Vollant A, Balarac G and Corre C 2017 *Journal of Turbulence* **18** 854–878
[38] van Ingen J and Kotsonis M 2011 A two-parameter method for en transition prediction *6th AIAA Theoretical Fluid Mechanics Conference* AIAA 2011-3928
[39] Yilmaz O C and et al 2017 Summary of the blind test campaign to predict the high reynolds number performance of du00-w210 airfoil *35th AIAA/ASME Wind Energy Symposium* AIAA 2017-0915

[40] Kevorkian J and Cole J D 1996 *Multiple scale and singular perturbation methods* (*Applied mathematical sciences* no 114) (Springer, New York)

[41] Veldman A 2008 Boundary layers Tech. rep. University of Groningen, Lecture Notes

[42] Morino L, Gennaretti M and Shen S 1995 *Meccanica* **30** 122–137

[43] Schlichting H and Gersten K 2017 *Boundary Layer Theory* (Springer-Verlag Berlin Heidelberg)

[44] Oleinik O and Samokhin V 1999 *Mathematical Models in Boundary Layer Turbulence* (Chapman Hall/CRC Press, Boca Raton)

[45] Blasius H 1950 The boundary layer in fluids with little friction Tech. rep. NACA TM 1256

[46] Falkner V and Skan S 1931 *Philosophical Magazine* **12** 865–896

[47] Farell P, Hegarty A, Miller J, O'riordan E and Shishkin G 2000 *Robust computational techniques for boundary layers* (Chapman Hall/CRC Press, Boca Raton)

[48] de Oliveira G, Kotsonis M and van Oudheusden B 2017 Laminar boundary layer flow with dbd plasma actuation: a similarity equation *Boundary and Interior Layers BAIL 2016* (*Springer Lecture Notes in Computational Science and Engineering* no 120)

[49] Emanuel G 2001 *Analytical fluid dynamics* (CRC Press, Boca Raton)

[50] Zagarola M V and Smits A J 1998 *Journal of Fluid Mechanics* **373**

[51] Chorin A J 1998 *Quarterly of applied mathematics*

[52] Castillo L and Wang X 2004 *Journal of Fluids Engineering*

[53] Clauser F 1954 *Journal of Aeronautical Sciences* **21**

[54] Bradshaw P 1969 The response of a constant-pressure turbulent boundary layer to the sudden application of an adverse pressure gradient Tech. rep. British ARC RM 3575

[55] Perry A 1966 *Journal of Fluid Mechanics* **26** 481–506

[56] Perry A, Marusic I and Jones M 1998 *Surveys in Fluid Mechanics IV* **23** 443–457

[57] Marusic I and Perry A 1995 *Journal of Fluid Mechanics* **298** 389–407

[58] Green J, Weeks D and Brooman J 1977 Prediction of turbulent boundary layers and wakes in compressible flow by a lag-entrainment method Tech. rep. British ARC RM 3791

[59] Ferriss D, Bradshaw P and Atwell N 1967 *Journal of Fluid Mechanics* **28** 593–616

[60] Coles D 1956 *Journal of Fluid Mechanics*

[61] Drela M and Giles M B 1987 *AIAA Journal* **25** 1347–1355

[62] Ramanujam G, Ozdemir H and Hoeijmakers H 2016 Improving airfoil drag prediction *34th AIAA/ASME Wind Energy Symposium* 2016-0748

[63] Timmer W 2009 An overview of naca 6-digit airfoil series characteristics with reference to airfoils for large wind turbine blades *47th AIAA Aerospace Sciences Meeting and Exhibit* 2009-268

[64] Mitchell T 1997 *Machine Learning* (McGraw-Hill, New York)

[65] Goodfellow I, Bengio Y and Courville A 2016 *Deep Learning* (MIT Press)

[66] Abbott I H, von Doenhoff A E and Stivers L 1945 Summary of airfoil data Tech. rep. NACA TR 824

[67] Siemens G P 1994 Naca report tr-824 - digitized

[68] Carmichael R 2011 Algorithm for calculating coordinates of cambered naca airfoils at specified chord locations *1st AIAA, Aircraft, Technology Integration, and Operations Forum*

[69] Kulfan B M 2007 A universal parametric geometry representation method - "cst" *45th AIAA Aerospace Sciences Meeting and Exhibit*

[70] Byrd R, Hribar M E and Nocedal J 1997 *ACM*

[71] Waltz R, Morales J, Nocedal J and Orban D 2006 *ACM*

[72] Timmer W and van Rooij R 1998 De invloed van een klepuitslag op de prestaties van profiel du 95-w-180 Tech. Rep. IW-98003R TU-Delft

[73] Eppler R and Somers D M 1980 A computer program for the design and analysis of low-speed airfoils Tech. rep. NASA TM-80210

[74] Perry A and Schofield W 1973 *Physics of Fluids* **16**

[75] Vinuesa R, Hosseini S M, Hanifi A, Henningson D S and Schlatter P 2017 *Flow, Turbulence and Combustion* **99** 613–641

[76] Ingber L 1995 *Polish Journal Control and Cybernetics*

[77] Hinton G, Srivastava N and Swersky K 2016 Rmsprop in neural networks for machine learning Tech. rep. University of Toronto